

PIM-GPT: A Hybrid Process-in-Memory Accelerator for Autoregressive Transformers

Yuting Wu[†], Ziyu Wang[†], Wei D. Lu

Department of Electrical Engineering and Computer Science, the University of Michigan, Ann Arbor, MI, USA

[†] Equal Contribution; listing order determined by random dice rolling.

Email: wuyt@umich.edu, ziwa@umich.edu, wluee@umich.edu

Abstract—Decoder-only Transformer models such as GPT have demonstrated superior performance in text generation, by autoregressively predicting the next token. However, the performance of GPT is bounded by low compute-to-memory-ratio and high memory access. Throughput-oriented architectures such as GPUs target parallel processing rather than sequential token generation, and are not efficient for GPT acceleration, particularly on-device inference applications. Process-in-memory (PIM) architectures can significantly reduce data movement and provide high computation parallelism, and are promising candidates to accelerate GPT inference.

In this work, we propose PIM-GPT that aims to achieve high throughput, high energy efficiency and end-to-end acceleration of GPT inference. PIM-GPT leverages DRAM-based PIM solutions to perform multiply-accumulate (MAC) operations on the DRAM chips, greatly reducing data movement. A compact application-specific integrated chip (ASIC) is designed and synthesized to initiate instructions to PIM chips and support data communication along with necessary arithmetic computations. At the software level, the mapping scheme is designed to maximize data locality and computation parallelism by partitioning a matrix among DRAM channels and banks to utilize all in-bank computation resources concurrently. We develop an event-driven clock-cycle accurate simulator to validate the efficacy of the proposed PIM-GPT architecture. Overall, PIM-GPT achieves 41–137 \times , 631–1074 \times speedup and 339–1085 \times , 890–1632 \times energy efficiency over GPU and CPU baseline, respectively, on 8 GPT models with up to 1.4 billion parameters.

Index Terms—Process-in-memory, GPT, Transformer, DRAM, Accelerator

I. INTRODUCTION

Attention-based Transformer models have revolutionized natural language processing (NLP) by capturing long-term dependencies in the input data [1]. Transformer models including GPT and BERT have demonstrated superior performance in many NLP tasks such as text generation [2] [3], text classification [4] [5] [6], and machine translation [7] [8] compared to convolution neural networks (CNNs) or recurrent neural networks (RNNs) [2] [9] [10]. GPT in particular has attracted widespread public interest. It is a decoder-only Transformer model that generates context in an autoregressive manner by producing a single token at one time [3]. However, the sequential processing feature of GPT will induce severe resource under-utilization of GPU, which is optimized for massively parallel processing. Additionally, GPT has two main features compared to CNNs: (1) extremely large model size and (2) low compute-to-memory-ratio. As shown in Figure 1,

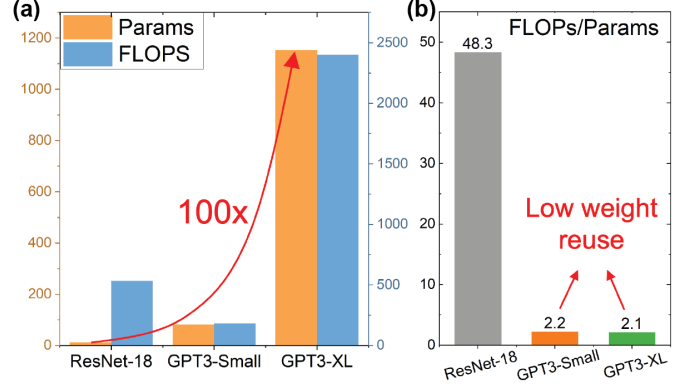


Fig. 1: (a) Parameter and computation cost comparison of GPTs and Resnet-18. (b) Operation/parameter ratios for CNN and GPT models.

the GPT3-XL model consists of 1.15 billion parameters [10], more than a hundred times higher than common CNNs such as ResNet-18 [11], while the arithmetic intensity per parameter (ops/parameter) is 2.1, much lower than 48.3 in ResNet-18.

These properties make it difficult to accelerate GPT models efficiently using architectures optimized for throughput such as GPUs. Several Transformer accelerators have been recently proposed to improve the performance of GPT inference [12] [13] [14]. However, these designs generally suffer from the following drawbacks: (1) expensive hardware overhead such as the usage of high-bandwidth memory (HBM) and dense in-memory logic; (2) model customization such as model and token pruning, which will make the architecture less flexible and cause accuracy loss; (3) incapability of long token length generation due to inefficient intermediate data management; (4) lack of end-to-end acceleration as most studies only focus on attention computation and feed-forward layers. Moreover, many of the existing Transformer accelerators are only designed for encoder-only model like BERT, instead of decoder-only models like GPT [15] [16] [17] [18] [19] [20] [21].

DRAM-based Process-in-memory (PIM) is a promising architecture to accelerate memory-bounded tasks [22] [23]. The high storage capacity of DRAM allows all model parameters to be stored. By adding compute elements to the DRAM chip, PIM can consume data locally and minimize external DRAM data access. Recent PIM developments show efficient

acceleration of MAC operation on DRAM chips [24] [25] [26] [27]. In comparison to conventional processor-centric architectures, implementing compute-logic near memory banks is a data-centric solution. However, only limited, low-density logic circuits can be fabricated on DRAM chips [28] [29]. Developments to date are limited to generic MAC operations, and efficient end-to-end PIM acceleration of GPT inference still needs to be developed.

In this work, we propose PIM-GPT, a complete solution for GPT inference acceleration. At the hardware level, PIM-GPT is a hybrid system that includes DRAM-based PIM chips to accelerate vector-matrix multiplication (VMM) near data and an application-specific integrated circuit (ASIC) to support other functions that are too expensive for PIM including necessary arithmetic computations, data communication and initiating instructions to the PIM chips. At the software level, mapping scheme is optimized to efficiently support the GPT dataflow. To accommodate the large model size and improve performance, the computation workloads are evenly distributed across PIM channels and banks to maximize the utilization of available computation resources and on-chip bandwidth. Multi-attention heads are concatenated to maximize data locality. Compared to existing Transformer accelerators [12] [13] [14], the proposed PIM-GPT supports large GPT models end-to-end without the need of expensive HBM, making it a practical solution for GPT acceleration on the edge. Benchmarking analysis shows the proposed PIM-GPT achieves state-of-the-art speedup and energy efficiency for GPT inference tasks.

In summary, the main contributions of our work are as follows:

- We design a hybrid architecture to accelerate the memory-bounded GPT inference end-to-end using GDDR6-based PIM with minimal changes to DRAM.
- We propose an optimized mapping scheme that maximizes data locality and distributes workloads across PIM channels and an ASIC to achieve high computation parallelism and efficiency.
- We analyze performance, efficiency, scalability and sensitivity of the proposed system through circuit synthesis and a clock-cycle accurate simulator.
- PIM-GPT achieves the state-of-art performance $41\text{--}137\times$, $631\text{--}1074\times$ speedup and $339\text{--}1085\times$, $890\text{--}1632\times$ energy efficiency over GPU and CPU baseline, respectively, for 8 GPT models with up to 1.4 billion parameters.

II. BACKGROUND AND MOTIVATION

A. Transformer Models

Figure 2 illustrates the typical structure of a Transformer model. Different from CNNs and RNNs, the Transformer model uses a self-attention mechanism that captures the relationship between different words in the whole sentence [1].

The original Transformer model consists of an encoder and a decoder, both containing N number of identical transformer blocks. Each block includes a self-attention module and a feed-forward network (FFN). Among them, BERT and GPT are the

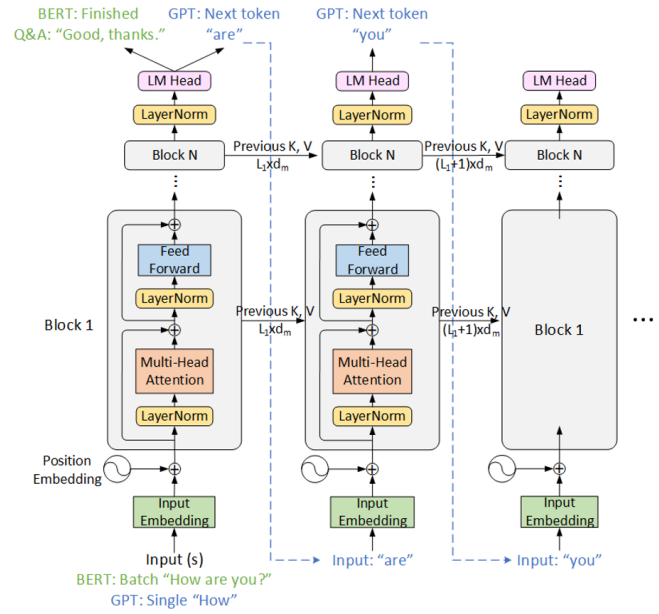


Fig. 2: Transformer model architectures of BERT and GPT.

two most popular language models. BERT is an encoder-only model, which processes all input tokens at once and attends to content in both directions [2]. In contrast, GPT is a decoder-only model, which typically handles a single token at one time and generates the next token in a sequential manner by attending to all previous tokens [10].

Despite the differences, these two models share similar blocks, as shown in Figure 2. For GPT, the input token is first transformed into a vector of dimension d_m by the input embedding layer, where d_m is the feature dimension of the model. Positional information of the token with respect to the sentence is also added to the input embeddings. The processed token is then fed into the Transformer blocks.

The input token is first multiplied with three linear transformation matrices ($W_{K,Q,V}$) to obtain Query (q), Key (k) and Value (v) vectors, where $W_K \in \mathbb{R}^{d_m \times d_k}$, $W_Q \in \mathbb{R}^{d_m \times d_k}$, $W_V \in \mathbb{R}^{d_m \times d_v}$. The current Key and Value vectors k , v are then concatenated to the key, value matrices computed from the previous inputs to form the updated Key, Value matrices. The q vector and Key, Value matrices are then passed to the self-attention head to capture the dependencies between tokens with the following equation:

$$\text{Attention}(q, K, V) = \text{softmax}\left(\frac{qK^T}{\sqrt{d_k}}\right)V \quad (1)$$

The scaled dot product between q and K^T is first computed to obtain the attention score, which measures the relation between the current token and all previous tokens. Then a softmax operation is applied to normalize the attention score between 0 and 1. In the next step, the attention score is multiplied with the value matrix to produce the head output. To allow the model to learn different relationships for each token, multi-head attention technique is adopted. The input vectors

are split across attention heads, and each chunk goes through a separate head in parallel. All head outputs are combined by a linear projection layer to produce the final attention output.

Following the multi-head attention, the attention output is fed into a FFN network, which consists of two fully-connected networks with Gaussian Error Linear Unit (GELU) activation function [30] in between. The attention and FFN layers both contain a layer normalization and a residual connection, as shown in Figure 2. The output from the attention block is then applied as inputs to the next attention block for subsequent processing, and the process is repeated through N attention blocks. Afterwards, a final output layer is used to predict the next token. The content is generated autoregressively by repeating this process until it reaches the required token length.

Unlike GPT, BERT processes all input tokens in parallel and produces the outputs at once. Therefore, the core computation is matrix-matrix multiplication, and the performance is computation-bounded. In contrast, for GPT the core computation is VMM and the arithmetic intensity is relatively low but the required memory access is high. As a result, throughput optimized architectures such as GPUs are not efficient for GPT inference, while PIM techniques that leverage compute capabilities on DRAM chips are promising for GPT inference hardware acceleration.

B. DRAM-based PIM

The conventional von Neumann architecture is a processor-centric design. Data need to be transferred across the memory hierarchy to the processor, which consumes about two orders of magnitude more energy than performing floating-point operation [25] [31]. Given these limitations, memory-centric computing architectures have been widely studied to accelerate memory-bounded tasks [22], such as genome sequence analysis [32] [33], graph processing [29] [34] and machine learning [35]. By moving processing units closer to data, PIM architectures enable data-centric, data-driven and data-aware designs. Amongst all PIM technologies, DRAM-based PIM architectures are promising candidates since DRAM is the mainstream memory in today's computing systems.

The DRAM bank is a two-dimensional array of memory cells with a 1T1C structure, as shown in the inset of Figure 3(c). The cell represents the binary values of "1" or "0" by the presence or absence of charge. When reading data from a DRAM bank, the wordline will be activated and data stream from an entire row will be offloaded to the row-buffer. Accessing and consuming existing data in the row-buffer is significantly efficient than from the array to the processor. However, the DRAM fabrication process is highly constrained for logic integration. It only contains three metal layers that severely limit the complexity of the circuit, and the transistors are $3\times$ slower than those in logic chips at the same node [36] [37]. Only until recent, advances in DRAM technology has made PIM design applicable. For example, Samsung proposed a function-in-memory DRAM (FIMDRAM) by adding programmable computing units between two banks of HBM [24]. Generally, HBM has been used in existing PIM architecture

designs [14] [29] [38] [39] [40] [41]. However, the high-cost associated with HBM makes it more suitable for servers instead of edge applications. Recently, SK Hynix announced GDDR6-based Accelerator-in-Memory (AiM) by implementing logic at the bank level to accelerate MAC operations and activation functions [26].

DRAM-based PIM can be divided into (1) process-using-memory (PUM) and (2) process-near-memory (PNM). The first approach supports computing in DRAM banks or sub-arrays. It can yield higher level of parallelism and less data movement. However, to enable in-bank computation, extensive modifications to the subarray architecture are needed [42] [43] [44]. Additionally, only a limited instruction set is supported. The second approach implements computation logic near DRAM banks and can take advantage of the large internal bandwidth [24] [26]. By balancing the computation logic design and bank organization, PNM based PIM can achieve both high-performance and energy efficiency.

C. Motivation

As shown in Figure 1, the computation primitive of GPT has low ops/parameter ratio and is memory-bounded since it processes and generates a single token at one time. Compared to computation-bounded models, the sequential feature of decoder cannot utilize parallel processing cores in GPU efficiently, particularly for inference tasks without batching. Recently, several Transformer accelerators have been proposed. Most of them mainly focus on the acceleration of matrix-matrix multiplication in encoder rather than the end-to-end model acceleration [15] [16] [17] [18] [19] [20] [21]. Only few considers GPT inference [12] [13] [14]. However, the use of HBM to increase memory bandwidth in these studies is expensive for edge inference applications.

PIM is a promising approach to relieve the memory bottleneck by storing matrix and performing computation in memory. However, at the hardware level, non-VMM operations are better performed in another chip to achieve efficient end-to-end GPT acceleration. At the software level, efficient workload distribution and dataflow management are required to fully exploit the advantage of PIM. The proposed PIM-GPT is such an end-to-end GPT accelerator with practical considerations in hardware implementation.

III. PIM-GPT ARCHITECTURE

A. System Overview

PIM-GPT is a memory-centric accelerator system aimed to support Transformer-based autoregressive token generation models including GPT. The PIM-GPT architecture is shown in Figure 3. The proposed system includes 8 GDDR6-based PIM channels with a custom designed ASIC. Each proposed PIM channel contains 16 memory banks, and only requires the integration of 16 on-chip MAC units and a shared global buffer (GB). Compared to HBM-PIM systems, GDDR6 DRAM does not rely on expensive 2.5D multi-die stack and through-silicon vias (TSVs), and is a low cost option for edge application.

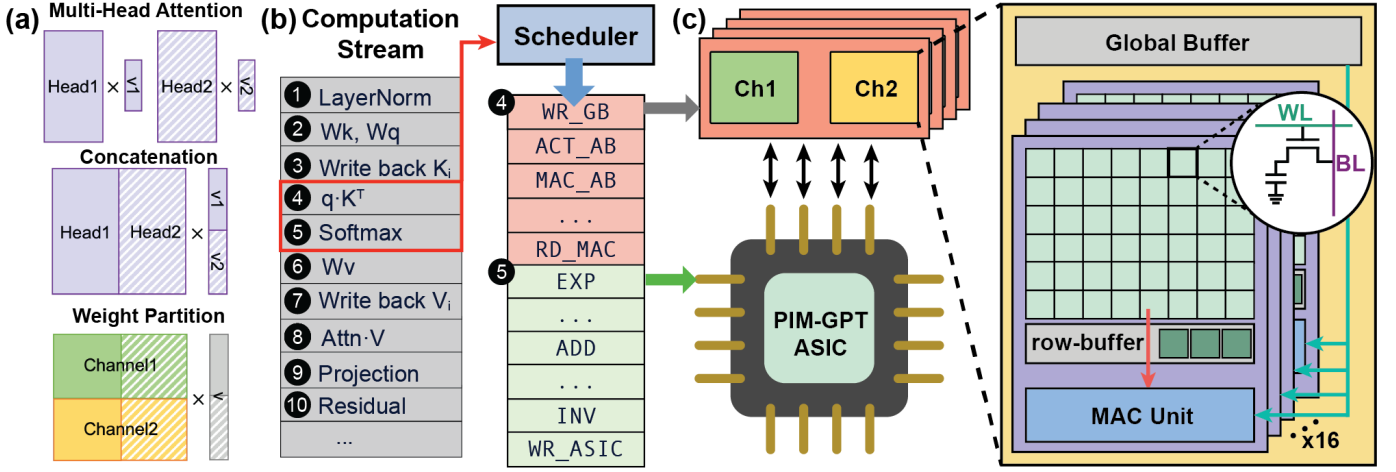


Fig. 3: PIM-GPT system overview. (a) Hardware-aware GPT model partition. (b) Compilation of computation stream to command stream. (c) PIM-GPT hardware architecture.

Our PIM design follows JEDEC standard [45] and operates at 1 GHz.

The design principle of PIM-GPT is to maximally leverage data locality and parallelism to achieve high system performance and energy efficiency. PIM-GPT supports end-to-end acceleration of large GPT models with long token length generation through: (1) hardware-aware model partition, (2) parallelism-aware instruction compilation and (3) throughput-aware dataflow between PIM and ASIC. As shown in Figure 3(a), weight values from multiple heads will be concatenated and distributed to multiple channels for parallel operation, which will be elaborated in Section IV. PIM-GPT is integrated with a data-triggered instruction scheduler, which compiles high-level computation streams of the model to DRAM/ASIC command streams. Figure 3(b) illustrates the compilation of ④ and ⑤ to command streams for PIM and ASIC, respectively. The hardware architecture is shown in Figure 3(c). In the hybrid architecture, the PIM chips execute VMM locally by broadcasting the vector stored in the GB and loading matrices from DRAM bank arrays to the MAC units. Only input/output vectors need to be transferred between PIM and ASIC instead of whole matrices. The ASIC computes non-VMM arithmetic computations, as well as manages data communication and intermediate data storage. All data in PIM-GPT are in bfloat16 (BF16) format, which preserves the approximate dynamic range of 32-bit floating point number to balance performance and accuracy.

B. GDDR6-based PIM Architecture

The GDDR6-based PIM architecture is shown in Figure 4. Unlike existing PIM designs [14] [29], our design only requires lightweight modifications to the conventional GDDR6 architecture. Integrating large SRAM buffer into DRAM is expensive and impractical. Therefore, only a 2 KB GB is added to each channel to store the input vector. The vector from GB can be broadcast to MAC units in all 16 banks to perform MAC simultaneously, as shown in Figure 4(a). When

the input length exceeds the GB size, partial MAC results will be computed and forwarded to the SRAM on ASIC, followed by downstream partial sum execution on the ASIC. Compared to writing back to DRAM, forwarding the subportion of VMM to ASIC reduces overall latency. Eliminating writing back also frees DRAM banks to perform subsequent parallel VMM. The data transmission rate of GDDR6 is 16 Gb/s/pin, and each channel has 16 pins leading to a total memory interface bandwidth of 32 GB/s.

The bank organization is identical to conventional DRAM architectures, as shown in Figure 4(b). Once a row address is decoded, the entire corresponding row will be activated and all stored data will be forwarded to the row buffer. Herein, if the bank is not closed (precharged), data will be preserved in the row buffer. Reading data from the row buffer is much faster than from the bank array, since it skips the long latency row activation step. Whether or not to precharge a row immediately after accessing the data is determined by the scheduling policy: open-row or close-row. Hence, using open-row policy can let the MAC unit consuming data much faster from DRAM if the data are properly mapped. In our optimized mapping scheme, the corresponding weights from DRAM banks share the same row addresses and the row hit rate is maximized, which will be discussed in Section IV.

Inside each bank, only multipliers and an adder tree are implemented for MAC operation. Similar architecture has been proven to be effective in prior designs [26] [46] [47]. During MAC operation, 16 vector values and corresponding weights are fetched from the GB and banks in the PIM channel, respectively. The 16 multipliers multiply the vector data with weights. The adder tree accumulates the multiplication results for downstream computation, as shown in Figure 4(c). The MAC units are operated in a pipelined fashion to maximize the throughput of the system, i.e. once the multiplication is done, the multipliers fetch the next chunk of vector and weight in the next clock cycle. The same principle is used for the adder stages. To minimize hardware cost and improve

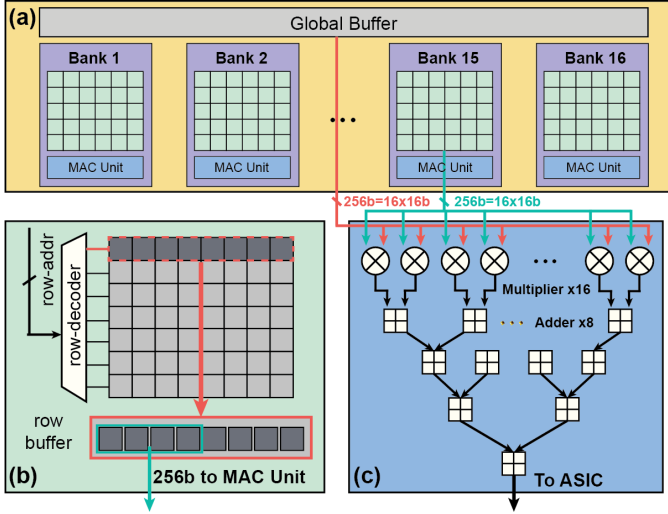


Fig. 4: DRAM PIM organization. (a) A channel is composed of a global buffer and 16 banks. A bank contains (b) a conventional DRAM bank and (c) a MAC unit with multipliers and an adder tree.

efficiency, PIM-GPT only performs VMM operations in the PIM while assigning all other computations, such as data bypassing, division and activation functions, to the ASIC. By doing so, the design allows the integration of lightweight MAC units to the DRAM chip to consume data locally without significantly sacrificing the memory capacity.

C. ASIC Architecture

The ASIC in PIM-GPT is used to manage data communication and support non-VMM arithmetic computations and intermediate data storage. The ASIC architecture is shown in Figure 5. Since VMM operations are performed in the PIM channels, data will only be read from DRAM PIM when a VMM operation is done and requires downstream computation or communication. The PIM channels communicate with the ASIC through memory bus and crossbar interconnects. The interconnects support data fetching from any DRAM channel and sending memory requests to a single channel or broadcasting data to all channels after packetizing data with address. Data read from PIM have two possible paths on the ASIC: (1) writing back to banks in other PIM channels, such as Key, Value matrices for subsequent VMM operations, and (2) going through computation blocks in the ASIC, such as layer normalization, softmax, etc.

If the data require downstream computation, they will be temporarily stored in the on-chip SRAM buffer. To further improve performance, PIM-GPT leverages pipelining between data transmission and ASIC computation to hide the data transmission latency caused by the limited GDDR6 bandwidth. The computation engine in ASIC can start execution when partial data are ready. The SRAM buffers and computation engines in the ASIC of the proposed PIM-GPT are designed for billion-parameter level models such as GPT3-XL. For smaller models or instructions that only utilize portions of the

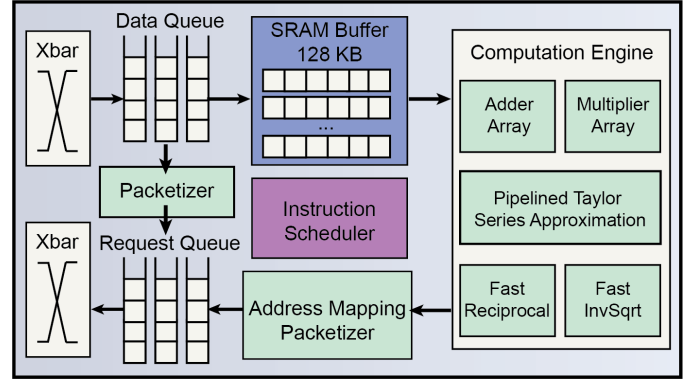


Fig. 5: ASIC architecture of the PIM-GPT system.

computation resources, power gating schemes will be applied to SRAM arrays or unused computation blocks to lower the ASIC power consumption.

PIM-GPT is designed for full stack autoregressive model acceleration. The computation engines on ASIC are responsible for computations that cannot be run as MACs, such as activation functions, layer normalization, softmax and partial sum. Details of the computation engine implementation will be discussed in the next sub-section.

D. ASIC Computation Block Design

The adders and multipliers in the computation engines follow the standard floating-point unit design to support summation and multiplication. For design reuse and performance considerations, other computation tasks are all implemented with approximation algorithms using only addition and multiplication to achieve the required precision.

Three functions that require approximation are shown in Equation 2–4: softmax, layer normalization and activation function GELU further approximated using Equation 4.

$$s(x_i) = \frac{e^{x_i}}{\sum_{j=1}^N e^j} \quad (2)$$

$$y = \frac{x - E[x]}{\sqrt{\text{Var}[x] + \epsilon}} \times \gamma + \beta \quad (3)$$

$$\begin{aligned} \text{GELU}(x) &= \frac{x}{2} \times [1 + \text{erf}(\frac{x}{\sqrt{2}})] \\ &= \frac{x}{2} \times [1 + \tanh \sqrt{2/\pi}(x + 0.044715 \times x^3)] \end{aligned} \quad (4)$$

The nonlinear function e^x , $\tanh x$, division and square root in these functions cannot be naively computed using addition and multiplication. Under given precision and data range, they can be efficiently approximated and converge in rapid iterations. Here e^x and $\tanh x$ are computed using Taylor series approximation with the first six items, which can be computed with addition and multiplication.

The division operation is computed by multiplying the numerator with the inverse of the denominator. Both the reciprocal and inverse square root operations can be calculated with

Algorithm 1: Newton-Raphson Division

Data: **BFloat16** $D = (S)M \times 2^E$
Result: **BFloat16** $\frac{1}{D}$
/* Scale by exponent subtraction */
1 $D' = D/2^{(E+1)}$
2 $X = \frac{48}{17} - \frac{32}{17} \times D'$
3 **for** $iter$ in $\lceil \log_2 \frac{P+1}{\log_2 17} \rceil$ **do**
4 | $X = X + X \times (1 - D' \times X)$
5 **end**
/* Scale the result */
6 $X' = X/2^{(E+1)}$

addition and multiplication following Newton’s method. A proper initial value is required to ensure the fast convergence. For reciprocal, we take advantage of Newton-Raphson division in Algorithm 1. The fast inverse square root algorithm is adopted from Quake III Arena’s source code [48], as shown in Algorithm 2.

The Newton-Raphson Division algorithm shown in Algorithm 1 is friendly for floating point numbers since it requires the input D to scale to a value close to 0, which can be easily done with exponent subtraction and mantissa shift in floating point data format. The P in line 3 is the precision of P binary places. Hence, for a 16-bit floating point number, it will take three iterations to get an accurate result. The fast inverse square root algorithm in Algorithm 2 unpacks the BF16 data into 16-bit integer data and padding 16-bit zeros to get an accurate approximation, followed by shift and subtraction from a constant. The pack step utilizes the 16 high bits of INT32 L' to assemble a BF16 data’s sign bit, exponent and mantissa. In the fast square root algorithm, it can converge in a single step iteration. Here we take a conservative two step iteration.

IV. PIM-GPT DATAFLOW

A. Overview

PIM-GPT distributes workloads among all PIM banks and ASIC efficiently. For VMM operation, the input vector is stored in the ASIC SRAM buffer and broadcast to the GB of all PIM channels. All MAC units will execute the same MAC instruction on different matrix partitions concurrently to fully utilize the PIM computation resources. The subvectors from channels will be sent back to ASIC for concatenation and downstream communication and computation. PIM-GPT implements the following techniques to coordinate workload between the PIM channels and the ASIC: (1) The partial outputs of VMM can be forwarded to the ASIC before the whole computation is completed, which effectively eliminates the data write back to DRAM banks; (2) When input vector length exceeds the GB size, SRAM buffer on the ASIC are reserved to store intermediate data and the ASIC will accumulate partial VMM results from DRAM; (3) Pipelining between data transmission and computation, i.e. the ASIC will

Algorithm 2: Fast Inverse Square Root

Data: **BFloat16** $D = (S)M \times 2^E$
Result: **BFloat16** $\frac{1}{\sqrt{D}}$
1 $D' = D \times 0.5$
/* Unpack data and pad with 0 */
2 **uint32_t** $L \leftarrow \{\text{unpack}(D'), 0x0000\}$
3 $L' = 0x5f3759df - L \gg 1$
/* Keep 16 high bits */
4 **BFloat16** $X \leftarrow \text{pack}(L')[31 : 16]$
5 **for** $iter$ in IterNum **do**
6 | $X = X \times (1.5 - D' \times X \times X)$
7 **end**

Algorithm 3: Model Mapping to PIM Banks

Data: Computation Graph; PIM Configuration
Result: Memory Mapping and Reservation
/* Map weights to PIM banks */
1 **for** $vmmBlock$ in *Computation Graph* **do**
2 | **if** $vmmBlock.multiHead$ **then**
3 | | $hitScore \leftarrow \text{maxRowHit}(nhead, ncol)$
4 | | $vmmBlock \leftarrow \text{concat}(hitScore, vmmBlock)$
5 | **end**
6 | $Mapping \leftarrow \text{maxParallel}(vmmBlock, nch, nbank)$
7 **end**
/* Reserve PIM bank rows for kv */
8 **for** $wrBlock$ in *Computation Graph* **do**
9 | **if** $block == write_k$ **then**
10 | | $hitScore \leftarrow \text{maxRowHit}(nhead, ncol, ltoken)$
11 | | $wrBlock \leftarrow \text{concat}(hitScore, wrBlock)$
12 | **end**
13 | $Mapping \leftarrow \text{Reserve}(wrBlock, ltoken, nch, nbank)$
14 **end**

start operations on partially received vector while the rest are in transmission.

The model mapping includes storing the weights to the allocated banks, and reserving space for the intermediate data (Key, Value matrices) for attention computation. To enhance the system performance, the mapping scheme is optimized to: (1) maximize row-hit rate by exploiting data locality; (2) increase computational parallelism by balancing the workload across DRAM banks; and (3) reduce latency by minimizing data movement. During runtime, the system automatically computes the bank address in the reserved space to write back the generated Key and Value vectors. The high-level description of the mapping scheme is shown in Algorithm 3.

B. Mapping Methods

Weight Mapping:

As shown in Figure 6, the mapping scheme leverages data locality and maximizes computation parallelism. Since commands such as activation (ACT) and precharge (PRE) are expensive, achieving a high row-hit rate is preferred. To this

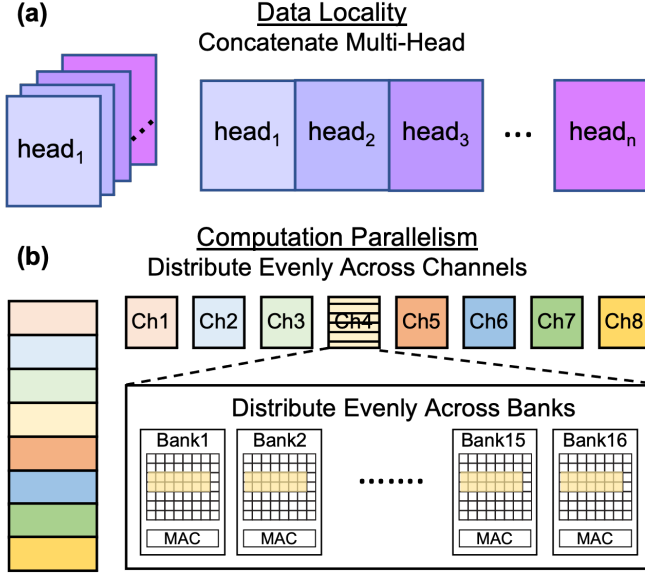


Fig. 6: Mapping strategy. (a) Concatenate multi-head to exploit data locality. (b) Distribute weight matrix (left) evenly across channels and banks to maximize computation parallelism.

end, matrix data used for MAC operations need to be mapped to consecutive physical DRAM cells. This approach means the corresponding row only needs to be activated once to transfer all required data to the row buffer, and the MAC units can keep consuming data already in the opened row to minimize ACT and PRE operations.

To take advantage of the data locality, it is desired that a row is fully mapped with data. However, a single attention head can be much smaller than the DRAM array dimension, e.g. head dimension of GPT2-XL is 64 while a row can store 1024 16-bit data. To maximize row hit rate, all attention heads in the same layer are concatenated to fill up the DRAM bank, as shown in Figure 6(a). To maximize the utilization of MAC units, the matrices are evenly distribute across PIM channels and banks, as shown in Figure 6(b). Figure 6(b) is a detailed example showing how W_v matrices are mapped through 8 PIM channels. First, attention heads in a layer are concatenated along column direction to form a larger matrix. The concatenated matrix is mapped following the row major approach and evenly distributed to all available channels, as indicated by the colors in Figure 6(a) and (b). Inside each channel, all 16 banks are mapped with a portion of the matrix and execute MAC operations in parallel. The computation is similar when it comes to VMM in the attention projection and FFN layers. This mapping scheme distributes weights evenly to achieve the highest possible DRAM channel-wise and bank-wise parallelism and run as many MAC units at the same time as possible.

Intermediate Data Memory Reservation:

Key and Value results need to be written back to the PIM banks and append to the existing Key and Value matrices. In the mapping stage, PIM-GPT reserves the required space in

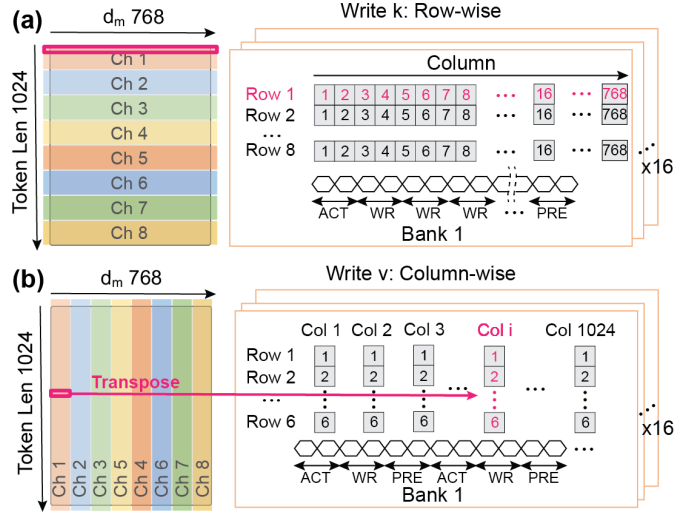


Fig. 7: (a) Write k row-wise. (b) Write v column-wise.

PIM banks for these intermediate data. The write back scheme of key and value results are shown in Figure 7(a) and (b), respectively. Key and Value write back are in row-major and column-major, respectively, since the transpose of Key matrix is required in Equation 1, while no transpose of Value matrix is required.

PIM-GPT exploits data locality during write. During run-time, the Key vectors produced by multi-attention heads will be concatenated together. As shown in Figure 7(a), Key vectors with length of 64 from 12 heads are concatenated to form a vector with length of 768, and written to the corresponding PIM bank row reserved for the current token, as highlighted by magenta in Figure 7(a). The write command can be executed consecutively after one ACT to store the whole Key vector, as shown in the timing diagram in Figure 7(a). The concatenated Key vectors produced by all token generation steps are evenly stored across all channels, as indicated by the color blocks in Figure 7(a). Within each channel, they are evenly distributed to all banks.

Value results are stored in column-major fashion. As shown in the timing diagram of Figure 7(b), in this case we can only write one data in an activated row. Then we close the row and move to the next row for the next data. Hence, data locality cannot be leveraged in Value result write back. To maximize the write throughput and computation parallelism in the subsequent VMM step, we distribute the Value matrix to all channels and banks, as shown in Figure 7(b).

V. SYSTEM EVALUATION

A. Evaluation Method

Hardware Configuration As DRAM fabrication process is highly constrained compared to the CMOS process, we refer AiM prototype reported from SK Hynix for area overhead evaluation. The area of one processing unit (PU) in AiM is 0.19 mm^2 [26]. Apart from MAC operation, the AiM PU includes bias addition and activation functions. For the pro-

posed PIM-GPT, these additional functions will be performed on the ASIC, and only MAC units are integrated on the DRAM chip resulting in less area overhead than the AiM PU design. All logic components of the ASIC are synthesized with SystemVerilog using Synopsys Design Compiler at TSMC 28nm HPC+ process node. Area and power of the logic components are obtained from the synthesis results. The area and power of SRAM buffer are extracted from the TSMC 28nm datasheet based on Synopsys Memory Compiler. The ASIC only consumes a core area of 0.64 mm^2 , and the peak power is 304.59 mW .

For DRAM energy benchmark analysis, we synthesized the optimized MAC units at 28 nm technology, followed by scaling the voltage to 1.25V to match the GDDR6 supply voltage [26]. Since routing is more complex in DRAM due to the limited metal layers compared to CMOS logic process, we conservatively multiply the power by 1.5, which comes to 149.29 mW for 16 MAC units. Since GDDR6 can be fabricated in 1nm technology [26], the actual power consumption is expected to be lower than this estimate. Table I lists the timing constraints and current values used to model the PIM behavior for each command. For PIM related commands, the timing constraints are obtained from [26]. For normal DRAM commands, we adopt GDDR5 timing constrains in [49] to make a conservative estimation due to the lack of detailed information of GDDR6. Similarly, the current values are obtained from DDR5 datasheet [50]. The system performance in latency and power efficiency is evaluated based on these conservative assumptions. Detailed hardware configuration is summarized in Table I.

Simulation Configuration To evaluate the PIM-GPT system performance, we developed an event-driven clock-cycle accurate simulator in C++ that models the system behavior at token generation runtime. The simulator takes the GPT model and system configuration as inputs for model mapping. The computation graph is compiled into an instruction sequence following the hardware constraints.

The PIM and ASIC behaviors are abstracted as state machines. The PIM hierarchy is organized as a tree structure at package, channel and bank levels. The PIM package node refers to the entire PIM portion that contains 8 PIM channels as child nodes. Each channel consists of 16 banks as child nodes. The state update will traverse down the tree from the root to the leaves. The same organization hierarchy can be found in other memory simulators, such as Ramulator [49].

The transition of states follows the timing constraints. At every clock cycle, the simulator checks the status of the ASIC and the PIM package. If both ASIC and PIM are in `Idle` state, the current instruction is completely consumed. It then fetches the next instruction, which will be decoded into command sequences. The ASIC or PIM will be put into `Process` state after the instruction is issued. The simulator will compute the future time `next_time` that the ASIC or relevant PIM banks will complete the triggered events based on the latency model. The simulator keeps track of the status of all hardware components. If the `CLK` reaches the `next_time`, the status

TABLE I: PIM-GPT Baseline Hardware Configuration.

Timing Constraint	tRCD=12ns, tRP=12ns, tCCD=1ns, tWR=12ns, tRFC=455ns, tREFI=6825ns
IDD	IDD2N=92mA, IDD3N=142mA, IDD0=122mA, IDD4R=530mA, IDD4W=470mA, IDD5B=277mA
GDDR6 Specification	Channel = 8, Banks/channel = 16, Capacity/channel = 4Gb, Row size = 2KB, Column number = 16k, Frequency = 1GHz, Pins = 16/channel, Data rate = 16Gb/s/pin
PIM	Buffer = 2KB/channel, MAC unit = 1/bank, Frequency = 1GHz, Power = 149.29mW
ASIC	Technology 28nm, Frequency = 1GHz, SRAM = 128KB, # of Adders = 256, # of Multipliers = 128, Area = 0.64mm^2 , Power = 304.59mW

of the corresponding node will be changed back to `Idle`.

Benchmark Analysis The performance and energy efficiency of the proposed PIM-GPT system are evaluated using the simulator and compared to GPU (NVIDIA T4) and CPU (Intel Xeon Gold 6154). 4 GPT2 and 4 GPT3 models with up to 1.4 billion parameters are implemented on the proposed PIM-GPT system, and used for the benchmark analysis. The simulator reports the total latency and the command sequences that are performed by the PIM channels and the ASIC. For PIM power, we multiply the IDD values consumed during each command with the corresponding latency and VDD, following the standard procedure [50] [51]. DRAM refresh operations are also included. The energy consumed by the PIM MAC units and by the ASIC are computed by multiplying the latency reported by the simulator with the synthesized power consumption.

We select NVIDIA T4 as the GPU benchmark as it also uses GDDR6 as memory for a fair comparison. For GPU, latency is recorded using `torch.cuda.Event()`, and power is measured with `pynvml`, which is a wrapper around the NVIDIA management library. The dynamic power consumption is tracked at each token generation and multiplied with the corresponding latency to get the total energy. For CPU characterization, we use python package `time.time()` for latency measurement and an open-source terminal tool `s-tui` for power monitor. In each measurement, we generate 1024 tokens and repeat 10 times, and report average energy and latency values.

B. Overall System Performance

Speedup As shown in Figure 8, the PIM-GPT system achieves remarkable performance improvements over GPU and CPU: $41\times$ to $137\times$ speedup over GPU T4 and $639\times$ to $1074\times$ speedup over CPU Xeon for the 8 GPT models. The high speedup originates from three aspects: (1) Memory bottleneck is effectively removed by performing the memory-intensive VMM operations inside PIM channel; (2) The mapping strategy maximizes computation parallelism and data locality; (3) Different workloads are efficiently distributed between PIM and ASIC. In comparison, GPU is not suitable for sequential token generation, since the large memory footprint

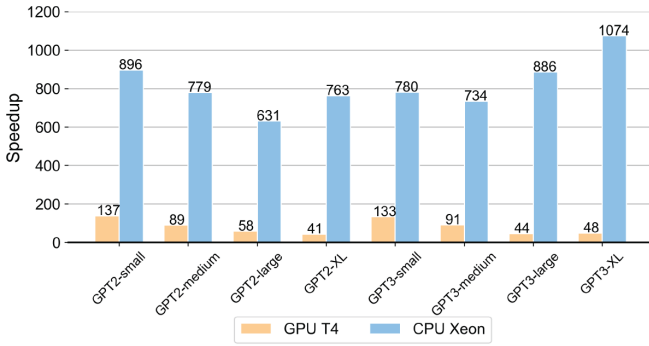


Fig. 8: Speedup w.r.t GPU and CPU.

and low data reuse rate under-utilize the GPU computation resources [13].

We also compare the PIM-GPT performance with previously reported Transformer accelerators, as shown in Table II. SpAtten [12] accelerates GPT2-medium by $35\times$ over GPU, and TransPIM [14] obtains similar speedup of $33\times$. Both ignore the layer normalization and residual connections in Transformer models. DFX [13] provides $3.2\times$ latency reduction on average. PIM-GPT achieves state-of-the-art performance with $89\times$ speedup over GPU. We also want to highlight that the PIM-GPT testing result is based on 1024 tokens, which cannot be supported by these prior prototypes.

Energy Efficiency Figure 9 shows that the PIM-GPT system achieves energy reduction of $339\times$ to $1085\times$ and $890\times$ to $1632\times$ over GPU and CPU, respectively. PIM-GPT effectively eliminates the energy consumption of DRAM data transmission by using PIM to locally consume data. Additionally, the mapping method leverages data locality and minimizes the row ACT and PRE operations that are energy consuming. The ASIC only contributes a very small fraction of the total system energy, but provides highly efficient arithmetic computations.

In comparison, DFX only achieves $3.99\times$ higher energy efficiency compared to the GPU baseline [13]. TransPIM reports $\sim 250\times$ energy reduction [14]. SpAtten reports $382\times$ over GPU [12], but only the attention layer is considered for energy consumption while others including FFN layers are not considered. Speedup and energy efficiency for the above mentioned accelerators are summarized in Table II.

C. Detailed Performance Analysis

The layerwise latency breakdown of GPT3-small and GPT3-XL in Figure 10 shows that VMM operations dominate the total execution time for PIM-GPT. All other arithmetic computations only account for 1.16% of total latency in GPT3-XL. For larger Transformer models, the improvement of PIM-GPT over GPU is reduced. This is because larger GPT models allow better utilization of GPU computation resources, while PIM has limited computation resources and the performance of PIM-GPT is computation-bounded. As a result, the gain over GPU is reduced when compared with smaller GPT models, although the performance gain ($>40\times$) is still significant.

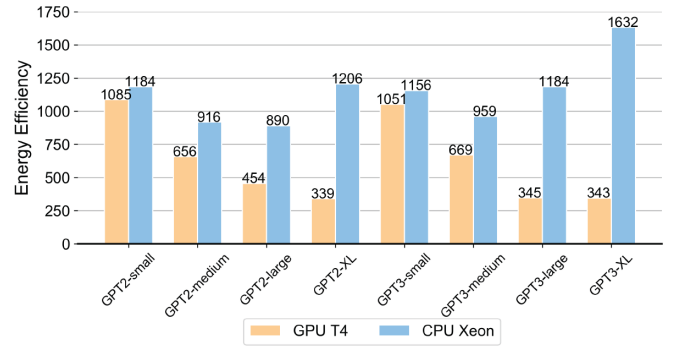


Fig. 9: Energy efficiency improvement w.r.t GPU and CPU.

The data locality is optimized during model mapping to reduce the memory access time and enhance the computation throughput. Figure 11(a) plots the row hit rates, achieving $\sim 98\%$ for all tested GPT models. For PIM-GPT, the VMM computation occurs on the same DRAM chip that stores the required weights and Key, Value vectors. Therefore, a significant amount of data movement can be eliminated. The data movement only happens when MAC results are transmitted to the ASIC for downstream processing or data synchronization. Figure 11(b) shows the data transfer reduction can be as large as $110\times$ to $259\times$. In PIM-GPT, data movement no longer becomes the bottleneck and consumes a very small proportion of the total latency, as illustrated by the layerwise breakdown in Figure 10.

TABLE II: Comparison with Other GPT Accelerators.

	SpAtten [12]	TransPIM [14]	DFX [13]	PIM-GPT
Memory	HBM	HBM	HBM+DDR	GDDR6
End-to-end	✗	✗	✓	✓
PIM	✗	✓	✗	✓
Data Type	INT	INT	FP16	BF16
Largest Model	GPT2-medium	GPT2-medium	GPT2-XL	GPT2/3-XL
Longest Token	32	-	128	8096
Speedup	$35\times$	$33\times$	$3.2\times$	$89\times$
Energy Efficiency	-	$\sim 260\times$	$3.99\times$	$618\times$

Notes: Speedup and energy efficiency are over GPU. PIM-GPT results are based on 1024 token generation. Other architectures generate the specified token lengths.

D. Sensitivity Study

We conduct sensitivity studies on the ASIC clock frequency and data transfer rate between PIM and ASIC to prove the robustness of the PIM-GPT design.

ASIC Frequency The PIM-GPT ASIC is designed with TSMC 28 nm technology at 1 GHz clock frequency. However, frequency scaling is an important technique to optimize the power consumption, especially for edge devices. We conduct

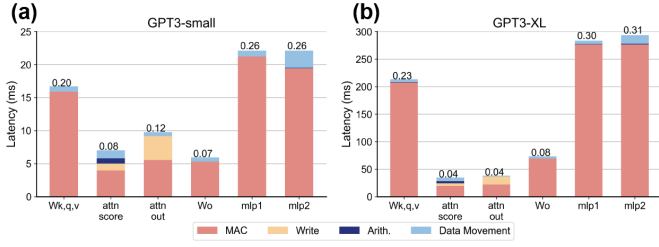


Fig. 10: Layer-wise latency breakdown of (a) GPT3-small and (b) GPT3-XL.

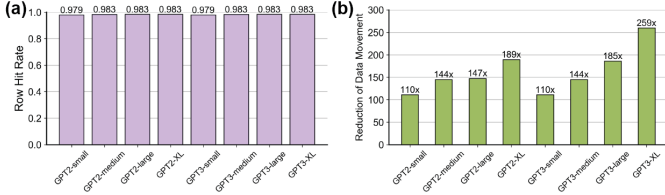


Fig. 11: (a) Row hit rate. (b) Reduction of data movement.

a sensitivity study of ASIC frequency by varying the latency setting in our simulator. Figure 12 shows the latency at different clock frequencies for the 8 GPT models, where the latency is normalized with respect to the 1 GHz results. Overall there is only a small latency increase when the ASIC frequency scales down from 1 GHz to 200 MHz for all models. Even when further scaling down the frequency to 100 MHz, which is 10 times slower than the baseline, the worst case only incurs a performance slowdown of 20%. Moreover, the larger models are less sensitive to the ASIC frequency scaling, since their operations are more dominated by VMM and the proportion of ASIC arithmetic computation is less than in smaller models. Therefore, the PIM-GPT design is not sensitive to ASIC clock frequency, which justifies its use for edge applications where power often needs to be optimized by reducing clock frequencies.

Data Transmission Rate The memory interface can be a bottleneck for many computation tasks, even for PIM implementations. In [27], SK Hynix reported that the performance of the 8-channel GDDR6-AiM system degrades by two orders of magnitude for matrix-vector multiplication (4096×4096) and handwritten digit recognition [$784 \times (4096 \times 4096 \times 4096) \times 10$, ReLU] tasks when the memory interface bandwidth is reduced from 300 Gb/s to 2 Gb/s [27]. When only accelerating fully connected layers in GPT models, the system with 4 channels experienced $\sim 3\times$ slowdown when memory interface bandwidth changes from 16 Gb/s to 2 Gb/s [52].

We test the PIM-GPT's sensitivity to the memory interface by changing the bandwidth configuration in our simulator. Figure 13 shows the latency as a function of memory interface bandwidth for 8 GPT models. When the memory interface bandwidth changes from 16 Gb/s to 2 Gb/s, the end-to-end GPT inference time is increased $\sim 1.5\times$ on average. That is $2\times$ better than reported in [52], where only VMM and GELU in GPT are considered. Even when the data transfer rate is

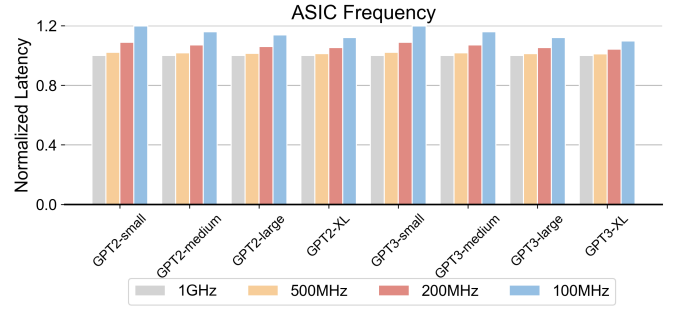


Fig. 12: Sensitivity of performance to ASIC clock frequency.

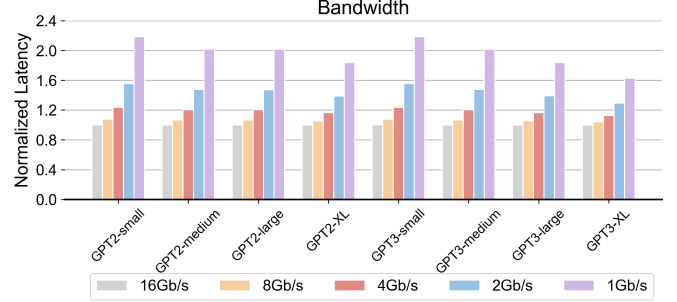


Fig. 13: Sensitivity of performance to data transfer rate.

decreased to 1 Gb/s, all models are slowed down by $\sim 2\times$ on average. These results show PIM-GPT is not sensitive to the memory interface bandwidth, since most data are consumed locally and the data transfer requirements are significantly reduced.

E. Long Token Support

As Transformer model sizes and token lengths increase, the required computation grows quadratically with the sequence length [53]. A lot of efforts have been devoted to reduce the computation and memory footprint for longer sequences by exploiting the sparsity and quantization of Transformer models [12] [54] [55]. Another approach is to approximate the softmax attention, e.g. linear Transformer [53], Performer [56] and spikeGPT [57], which reduces the space complexity of attention from quadratic to linear. However, approximations can impact the accuracy of large Transformer models, while dynamic pruning at runtime adds hardware design complexity [12] [46]. The proposed PIM-GPT mapping scheme evenly distributes model parameters across PIM channels, therefore can support more than 8k token generation for GPT3-XL. Figure 14 shows normalized latency of different token lengths with respect to 1k tokens.

F. Scalability

Since the performance of PIM-GPT is computation-bounded, the latency can be reduced by adding more computation resources. Figure 15 evaluates the scalability of the system. When the computation throughput of the MAC unit is increased from processing 16 MACs to 64 MACs at a time,

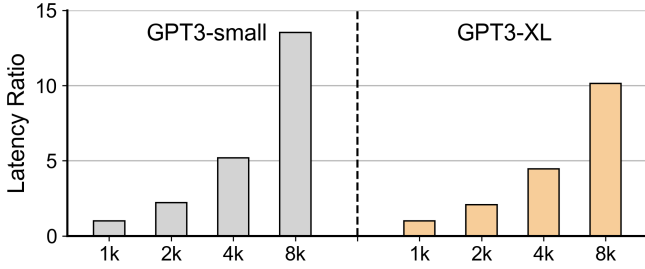


Fig. 14: PIM-GPT latency with increased token length.

the latency is reduced by $1.8\times$ and $2.0\times$ for GPT3-small and GPT3-XL, respectively, as shown in Figure 15(a). The speedup is sub-linear. This is because when PIM performs MAC operations on a bank row, the row needs to be activated and precharged, which consumes a significant amount of time. We also evaluate performance enhancement by increasing computation parallelism, as shown in Figure 15(b). More memory channels can be attached to the ASIC with relatively minor modifications to the ASIC data port. The improvement scales almost linearly with the number of channels. The speedup slightly reduces for longer sequences, because longer sequence requires more arithmetic computation for ASIC to process.

VI. RELATED WORK

Process-in-Memory DRAM-based PIM is one of the most promising technologies to accelerate data-intensive computing tasks. UPMEM is the first reported PIM product using standard DIMM modules, with a large number of processors combined with DRAM chips [36] [37]. However, the throughput per PU is 4 GOPS and it only supports INT8 data type. DRAM vendors including Samsung [24] [25] and SK Hynix [26] [27] have recently announced DRAM-based PIM technologies. Samsung’s PIM architecture is based on HBM2, which offers high bandwidth of 307.2 GBps to tackle data intensive tasks. The design integrates PIM dies on a buffer die through TSV. Inside each PIM die, a PU is shared by two banks, operating at 9.6GFLOPS per PU. However, the high cost of HBM limits the application to server level. SK Hynix’s GDDR6-based PIM prototype, Accelerator-in-Memory (AiM), uses the standard GDDR6 interface. AiM supports VMM with high throughput of 32GFLOPS per PU. However, AiM alone cannot accelerate end-to-end applications due to the limited logic and arithmetic units that are fabricated on DRAM chips. For example, AiM cannot support complex interlayer functions such as softmax, normalization, and residual connections. Compared to AiM, PIM-GPT reduces PIM cost by limiting PIM only to VMM operations, and performs the other arithmetic and control functions in a separate ASIC with optimized mapping and dataflow design to allow efficient end-to-end GPT acceleration.

GPT Accelerators Recently, several Transformer accelerators have been proposed. Most of them target computation-intensive encoder models [15] [16] [17] [18] and are not well-

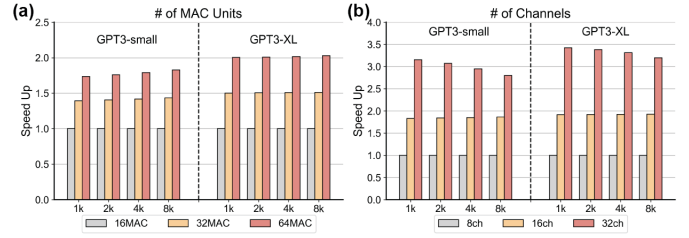


Fig. 15: Scalability of PIM-GPT with increased number of (a) MAC units and (b) channels.

optimized for the memory-bounded GPT inference. Few works accelerate GPT token generation tasks [12] [13] [14]. They all rely on the high cost HBM. These architectures are not well-optimized for the memory-bounded GPT inference. Hence, the performance improvement is limited. DFX [13] partitions the GPT models to multiple FPGAs to leverage parallel computation, but does not reduce the data load/store and requires both DDR4 and HBM for GPT models. SpAtten [12] involves algorithmic methods such as pruning and quantization to reduce memory overhead. However, these methods inevitably reduce the model inference accuracy. SpAtten also only speeds up the attention mechanism in Transformer. TransPIM [14] takes advantage of PIM and proposes a token based dataflow requiring a large ring broadcast buffer (2kb) per bank to store temporary data and direct link between two adjacent banks. This design requires subarray-level modification that adds significant overhead to the DRAM chip. Arithmetic computations like layernorm and residual connections are not considered either. Moreover, these prior works only demonstrate acceleration for limited token length. The proposed PIM-GPT optimizes the workload distribution to exploit the benefits of both PIM and ASIC to achieve fast end-to-end GPT acceleration on the edge.

VII. CONCLUSION

In this work, we propose a hybrid hardware system, PIM-GPT, to accelerate the memory-bounded GPT token generation tasks. PIM-GPT consists of GDDR6-based PIM chips and a lightweight ASIC chip to support end-to-end GPT acceleration. Model mapping and workload distribution are optimized to maximize computation parallelism and data locality. The proposed system achieves $41\text{--}137\times$, $631\text{--}1074\times$ speedup and $339\text{--}1085\times$, $890\text{--}1632\times$ energy efficiency over GPU and CPU on 8 GPT models. We highlight that the design only requires light modifications to the DRAM architecture, which offers a practical solution for edge applications. PIM-GPT exhibits other favorable characteristics, including low sensitivity to ASIC clock frequency and memory interface specs, capable of long token generation and excellent scalability.

ACKNOWLEDGEMENTS

This work was supported in part by the National Science Foundation through Award CCF-1900675.

REFERENCES

- [1] A. Vaswani, N. Shazeer, N. Parmar, J. Uszkoreit, L. Jones, A. N. Gomez, L. Kaiser, and I. Polosukhin, "Attention is all you need," *Advances in neural information processing systems*, vol. 30, 2017.
- [2] J. Devlin, M.-W. Chang, K. Lee, and K. Toutanova, "Bert: Pre-training of deep bidirectional transformers for language understanding," *arXiv preprint arXiv:1810.04805*, 2018.
- [3] R. OpenAI, "Gpt-4 technical report," *arXiv*, pp. 2303–08 774, 2023.
- [4] C. Sun, X. Qiu, Y. Xu, and X. Huang, "How to fine-tune bert for text classification?" in *Chinese Computational Linguistics: 18th China National Conference, CCL 2019, Kunming, China, October 18–20, 2019, Proceedings 18*. Springer, 2019, pp. 194–206.
- [5] W.-C. Chang, H.-F. Yu, K. Zhong, Y. Yang, and I. S. Dhillon, "Taming pretrained transformers for extreme multi-label text classification," in *Proceedings of the 26th ACM SIGKDD international conference on knowledge discovery & data mining*, 2020, pp. 3163–3171.
- [6] S. Garg and G. Ramakrishnan, "Bae: Bert-based adversarial examples for text classification," *arXiv preprint arXiv:2004.01970*, 2020.
- [7] Q. Wang, B. Li, T. Xiao, J. Zhu, C. Li, D. F. Wong, and L. S. Chao, "Learning deep transformer models for machine translation," *arXiv preprint arXiv:1906.01787*, 2019.
- [8] S. Yao and X. Wan, "Multimodal transformer for multimodal machine translation," in *Proceedings of the 58th annual meeting of the association for computational linguistics*, 2020, pp. 4346–4350.
- [9] A. Radford, J. Wu, R. Child, D. Luan, D. Amodei, I. Sutskever *et al.*, "Language models are unsupervised multitask learners," *OpenAI blog*, vol. 1, no. 8, p. 9, 2019.
- [10] T. Brown, B. Mann, N. Ryder, M. Subbiah, J. D. Kaplan, P. Dhariwal, A. Neelakantan, P. Shyam, G. Sastry, A. Askell *et al.*, "Language models are few-shot learners," *Advances in neural information processing systems*, vol. 33, pp. 1877–1901, 2020.
- [11] K. He, X. Zhang, S. Ren, and J. Sun, "Deep residual learning for image recognition," in *Proceedings of the IEEE conference on computer vision and pattern recognition*, 2016, pp. 770–778.
- [12] H. Wang, Z. Zhang, and S. Han, "Spatten: Efficient sparse attention architecture with cascade token and head pruning," in *2021 IEEE International Symposium on High-Performance Computer Architecture (HPCA)*. IEEE, 2021, pp. 97–110.
- [13] S. Hong, S. Moon, J. Kim, S. Lee, M. Kim, D. Lee, and J.-Y. Kim, "Dfx: A low-latency multi-fpga appliance for accelerating transformer-based text generation," in *2022 55th IEEE/ACM International Symposium on Microarchitecture (MICRO)*. IEEE, 2022, pp. 616–630.
- [14] M. Zhou, W. Xu, J. Kang, and T. Rosing, "Transpim: A memory-based acceleration via software-hardware co-design for transformer," in *2022 IEEE International Symposium on High-Performance Computer Architecture (HPCA)*. IEEE, 2022, pp. 1071–1085.
- [15] T. J. Ham, S. J. Jung, S. Kim, Y. H. Oh, Y. Park, Y. Song, J.-H. Park, S. Lee, K. Park, J. W. Lee *et al.*, "A³: Accelerating attention mechanisms in neural networks with approximation," in *2020 IEEE International Symposium on High Performance Computer Architecture (HPCA)*. IEEE, 2020, pp. 328–341.
- [16] T. J. Ham, Y. Lee, S. H. Seo, S. Kim, H. Choi, S. J. Jung, and J. W. Lee, "Elsa: Hardware-software co-design for efficient, lightweight self-attention mechanism in neural networks," in *2021 ACM/IEEE 48th Annual International Symposium on Computer Architecture (ISCA)*. IEEE, 2021, pp. 692–705.
- [17] H. Jang, J. Kim, J.-E. Jo, J. Lee, and J. Kim, "Mnnfast: A fast and scalable system architecture for memory-augmented neural networks," in *Proceedings of the 46th International Symposium on Computer Architecture*, 2019, pp. 250–263.
- [18] A. H. Zadeh, I. Edo, O. M. Awad, and A. Moshovos, "Gobo: Quantizing attention-based nlp models for low latency and energy efficient inference," in *2020 53rd Annual IEEE/ACM International Symposium on Microarchitecture (MICRO)*. IEEE, 2020, pp. 811–824.
- [19] H. Wang, H. Xu, Y. Wang, and Y. Han, "Cta: Hardware-software co-design for compressed token attention mechanism," in *2023 IEEE International Symposium on High-Performance Computer Architecture (HPCA)*. IEEE, 2023, pp. 429–441.
- [20] J. Dass, S. Wu, H. Shi, C. Li, Z. Ye, Z. Wang, and Y. Lin, "Vitality: Unifying low-rank and sparse approximation for vision transformer acceleration with a linear taylor attention," in *2023 IEEE International Symposium on High-Performance Computer Architecture (HPCA)*. IEEE, 2023, pp. 415–428.
- [21] H. You, Z. Sun, H. Shi, Z. Yu, Y. Zhao, Y. Zhang, C. Li, B. Li, and Y. Lin, "Vitcod: Vision transformer acceleration via dedicated algorithm and accelerator co-design," in *2023 IEEE International Symposium on High-Performance Computer Architecture (HPCA)*. IEEE, 2023, pp. 273–286.
- [22] O. Mutlu, "Memory-centric computing," *arXiv preprint arXiv:2305.20000*, 2023.
- [23] S. Ghose, A. Boroumand, J. S. Kim, J. Gómez-Luna, and O. Mutlu, "Processing-in-memory: A workload-driven perspective," *IBM Journal of Research and Development*, vol. 63, no. 6, pp. 3–1, 2019.
- [24] Y.-C. Kwon, S. H. Lee, J. Lee, S.-H. Kwon, J. M. Ryu, J.-P. Son, O. Seongil, H.-S. Yu, H. Lee, S. Y. Kim *et al.*, "25.4 a 20nm 6gb function-in-memory dram, based on hbm2 with a 1.2 tflops programmable computing unit using bank-level parallelism, for machine learning applications," in *2021 IEEE International Solid-State Circuits Conference (ISSCC)*, vol. 64. IEEE, 2021, pp. 350–352.
- [25] S. Lee, S.-h. Kang, J. Lee, H. Kim, E. Lee, S. Seo, H. Yoon, S. Lee, K. Lim, H. Shin *et al.*, "Hardware architecture and software stack for pim based on commercial dram technology: Industrial product," in *2021 ACM/IEEE 48th Annual International Symposium on Computer Architecture (ISCA)*. IEEE, 2021, pp. 43–56.
- [26] S. Lee, K. Kim, S. Oh, J. Park, G. Hong, D. Ka, K. Hwang, J. Park, K. Kang, J. Kim *et al.*, "A 1ynm 1.25 v 8gb, 16gb/s/pin gddr6-based accelerator-in-memory supporting 1tflops mac operation and various activation functions for deep-learning applications," in *2022 IEEE International Solid-State Circuits Conference (ISSCC)*, vol. 65. IEEE, 2022, pp. 1–3.
- [27] D. Kwon, S. Lee, K. Kim, S. Oh, J. Park, G.-M. Hong, D. Ka, K. Hwang, J. Park, K. Kang *et al.*, "A 1ynm 1.25 v 8gb 16gb/s/pin gddr6-based accelerator-in-memory supporting 1tflops mac operation and various activation functions for deep learning application," *IEEE Journal of Solid-State Circuits*, vol. 58, no. 1, pp. 291–302, 2022.
- [28] A. Yazdanbakhsh, C. Song, J. Sacks, P. Lotfi-Kamran, H. Esmailzadeh, and N. S. Kim, "In-dram near-data approximate acceleration for gpus," in *Proceedings of the 27th International Conference on Parallel Architectures and Compilation Techniques*, 2018, pp. 1–14.
- [29] X. Xie, Z. Liang, P. Gu, A. Basak, L. Deng, L. Liang, X. Hu, and Y. Xie, "Spacea: Sparse matrix vector multiplication on processing-in-memory accelerator," in *2021 IEEE International Symposium on High-Performance Computer Architecture (HPCA)*. IEEE, 2021, pp. 570–583.
- [30] D. Hendrycks and K. Gimpel, "Gaussian error linear units (gelus)," *arXiv preprint arXiv:1606.08415*, 2016.
- [31] S. W. Keckler, W. J. Dally, B. Khailany, M. Garland, and D. Glasco, "Gpus and the future of parallel computing," *IEEE micro*, vol. 31, no. 5, pp. 7–17, 2011.
- [32] H. Mao, M. Alser, M. Sadrosadati, C. Firtina, A. Baranwal, D. S. Cali, A. Manglik, N. A. Alserr, and O. Mutlu, "Genpip: In-memory acceleration of genome analysis via tight integration of basecalling and read mapping," in *2022 55th IEEE/ACM International Symposium on Microarchitecture (MICRO)*. IEEE, 2022, pp. 710–726.
- [33] N. M. Ghiasi, J. Park, H. Mustafa, J. Kim, A. Olgun, A. Gollwitzer, D. S. Cali, C. Firtina, H. Mao, N. A. Alserr *et al.*, "Genstore: A high-performance and energy-efficient in-storage computing system for genome sequence analysis," *arXiv preprint arXiv:2202.10400*, 2022.
- [34] L. Song, Y. Zhuo, X. Qian, H. Li, and Y. Chen, "Graphr: Accelerating graph processing using reram," in *2018 IEEE International Symposium on High Performance Computer Architecture (HPCA)*. IEEE, 2018, pp. 531–543.
- [35] J. Gómez-Luna, Y. Guo, S. Brocard, J. Legriel, R. Cimadomo, G. F. Oliveira, G. Singh, and O. Mutlu, "Evaluating machine learning workloads on memory-centric computing systems," in *2023 IEEE International Symposium on Performance Analysis of Systems and Software (ISPASS)*. IEEE, 2023, pp. 35–49.
- [36] F. Devaux, "The true processing in memory accelerator," in *2019 IEEE Hot Chips 31 Symposium (HCS)*. IEEE Computer Society, 2019, pp. 1–24.
- [37] J. Gómez-Luna, I. El Hajj, I. Fernandez, C. Giannoula, G. F. Oliveira, and O. Mutlu, "Benchmarking a new paradigm: Experimental analysis and characterization of a real processing-in-memory system," *IEEE Access*, vol. 10, pp. 52 565–52 608, 2022.
- [38] J. H. Kim, S.-h. Kang, S. Lee, H. Kim, W. Song, Y. Ro, S. Lee, D. Wang, H. Shin, B. Phuah *et al.*, "Aquabolt-xl: Samsung hbm2-pim with in-

- memory processing for ml accelerators and beyond,” in *2021 IEEE Hot Chips 33 Symposium (HCS)*. IEEE, 2021, pp. 1–26.
- [39] S. Kang, S. Lee, B. Kim, H. Kim, K. Sohn, N. S. Kim, and E. Lee, “An fpga-based rnn-t inference accelerator with pim-hbm,” in *Proceedings of the 2022 ACM/SIGDA International Symposium on Field-Programmable Gate Arrays*, 2022, pp. 146–152.
- [40] D. Niu, S. Li, Y. Wang, W. Han, Z. Zhang, Y. Guan, T. Guan, F. Sun, F. Xue, L. Duan *et al.*, “184qps/w 64mb/mm 2 3d logic-to-dram hybrid bonding with process-near-memory engine for recommendation system,” in *2022 IEEE International Solid-State Circuits Conference (ISSCC)*, vol. 65. IEEE, 2022, pp. 1–3.
- [41] M. Orenes-Vera, E. Tureci, D. Wentzlaff, and M. Martonosi, “Dalorex: A data-local program execution and architecture for memory-bound applications,” in *2023 IEEE International Symposium on High-Performance Computer Architecture (HPCA)*. IEEE, 2023, pp. 718–730.
- [42] S. Li, D. Niu, K. T. Malladi, H. Zheng, B. Brennan, and Y. Xie, “Drise: A dram-based reconfigurable in-situ accelerator,” in *Proceedings of the 50th Annual IEEE/ACM International Symposium on Microarchitecture*, 2017, pp. 288–301.
- [43] F. Gao, G. Tziatzoulis, and D. Wentzlaff, “Computedram: In-memory compute using off-the-shelf drams,” in *Proceedings of the 52nd annual IEEE/ACM international symposium on microarchitecture*, 2019, pp. 100–113.
- [44] M. Jeong and W. Jung, “Mac-do: Charge based multi-bit analog in-memory accelerator compatible with dram using output stationary mapping,” *arXiv preprint arXiv:2207.07862*, 2022.
- [45] JEDEC. Graphics double data rate (gddr6) sgram standard. [Online]. Available: <https://www.jedec.org/standards-documents/docs/jesd250d>
- [46] Z. Fan, Q. Zhang, P. Abillama, S. Shoori, C. Lee, D. Blaauw, H.-S. Kim, and D. Sylvester, “Taskfusion: An efficient transfer learning architecture with dual delta sparsity for multi-task natural language processing,” in *Proceedings of the 50th Annual International Symposium on Computer Architecture*, 2023, pp. 1–14.
- [47] M. He, C. Song, I. Kim, C. Jeong, S. Kim, I. Park, M. Thottethodi, and T. Vijaykumar, “Newton: A dram-maker’s accelerator-in-memory (aim) architecture for machine learning,” in *2020 53rd Annual IEEE/ACM International Symposium on Microarchitecture (MICRO)*. IEEE, 2020, pp. 372–385.
- [48] Fast inverse square root. [Online]. Available: https://en.wikipedia.org/wiki/Fast_inverse_square_root
- [49] Y. Kim, W. Yang, and O. Mutlu, “Ramulator: A fast and extensible dram simulator,” *IEEE Computer architecture letters*, vol. 15, no. 1, pp. 45–49, 2015.
- [50] Micron. 16gb ddr5 sdram addendum. [Online]. Available: https://media-www.micron.com/-/media/client/global/documents/products/data-sheet/dram/ddr5/16gb_ddr5_sdram_diereva.pdf
- [51] S. Ghose, A. G. Yaglikçi, R. Gupta, D. Lee, K. Kudrolli, W. X. Liu, H. Hassan, K. K. Chang, N. Chatterjee, A. Agrawal *et al.*, “What your dram power models are not telling you: Lessons from a detailed experimental study,” *Proceedings of the ACM on Measurement and Analysis of Computing Systems*, vol. 2, no. 3, pp. 1–41, 2018.
- [52] Y. Kwon, K. Vladimir, N. Kim, W. Shin, J. Won, M. Lee, H. Joo, H. Choi, G. Kim, B. An *et al.*, “System architecture and software stack for gddr6-aim,” in *2022 IEEE Hot Chips 34 Symposium (HCS)*. IEEE, 2022, pp. 1–25.
- [53] A. Katharopoulos, A. Vyas, N. Pappas, and F. Fleuret, “Transformers are rnns: Fast autoregressive transformers with linear attention,” in *International conference on machine learning*. PMLR, 2020, pp. 5156–5165.
- [54] I. Beltagy, M. E. Peters, and A. Cohan, “Longformer: The long-document transformer,” *arXiv preprint arXiv:2004.05150*, 2020.
- [55] Y. Tay, M. Dehghani, D. Bahri, and D. Metzler, “Efficient transformers: A survey. arxiv 2020,” *arXiv preprint arXiv:2009.06732*.
- [56] K. Choromanski, V. Likhoshesterov, D. Dohan, X. Song, A. Gane, T. Sarlos, P. Hawkins, J. Davis, A. Mohiuddin, L. Kaiser *et al.*, “Rethinking attention with performers,” *arXiv preprint arXiv:2009.14794*, 2020.
- [57] R.-J. Zhu, Q. Zhao, and J. K. Eshraghian, “Spikept: Generative pre-trained language model with spiking neural networks,” *arXiv preprint arXiv:2302.13939*, 2023.